Available online at www.sciencedirect.com
ScienceDirect
International Journal of Heat and Mass Transfer 49 (2006) 4839–4849
International Journal of HEAT and MASS TRANSFER
www.elsevier.com/locate/ijhmt

Thermodynamic optimization of tree-shaped flow geometries with constant channel wall temperature

V.D. Zimparov [a,*], A.K. da Silva [b], A. Bejan [c]

[a] Department of Mechanical Engineering, Gabrovo Technical University, 4 Hadji Dimitar Str., 5300 Gabrovo, Bulgaria
[b] Department of Mechanical Engineering, University of Hawaii, Manoa, Honolulu, HI 96822, USA
[c] Department of Mechanical Engineering and Materials Science, Duke University, Box 90300, Durham, NC 27708-0300, USA

Received 5 January 2006; received in revised form 15 May 2006
Available online 10 August 2006

Abstract

In this paper, we optimize the performance of several classes of simple flow systems consisting of T- and Y-shaped assemblies of ducts, channels and streams. In each case, the objective is to identify the geometric configuration that maximizes performance subject to several global constraints. Maximum thermodynamic performance is achieved by minimization of the entropy generated in the assemblies. The boundary condition is fixed temperature of the channel wall. The flow is assumed laminar and fully developed. Every geometrical detail of the optimized structure is deduced from the constructal law. Performance evaluation criterion is proposed for evaluation and comparison of the effectiveness of different tree-shaped design heat exchangers. This criterion takes into account and compare the entropy generated in the system with heat transfer performance achieved.

Keywords: Constructal theory; Thermodynamic optimization; Entropy generation minimization

1. Introduction

Among the more recent methods that have become established in thermal engineering, thermodynamic optimization has the objective of improving the global performance of the system subject to specified global constraints. Thermodynamic optimization is useful as a first step, for orientation in the search of tradeoffs that govern the geometrical configuration of the system. Tree networks were brought to heat transfer by constructal theory [1,2] and now represent a new trend in the optimization and miniaturization of heat transfer devices [1–6], mass exchangers [7,8], chemical reactors [9], and fuel cells [10–12]. Tree-shaped architectures promise a more judicious use of the available space: higher densities of heat and mass transfer and chemical reactions, and a more uniform volumetric distribution of transport processes. The fundamental study of the optimization of tree-shaped architectures also sheds light on the common design principles of engineered and natural flow systems.

In design, and in society in general, space is at a premium. This is why the interest in performance at smaller and smaller scales is natural, and will continue. The miniaturization revolution means not only that the smallest identifiable volume element (the *elemental* system [1]) is becoming smaller, but also that larger and larger numbers of such elements must inhabit the microscopic device that they serve. The smaller the elements, and the larger their number, the greater the complexity of the structure. Packing the system with smaller, more powerful and more numerous elemental systems is a necessary first step. The challenge is not only to find geometric arrangements to connect the currents that access the elemental systems, but to *optimize* each connection such that, ultimately, each design choice is reflected in an increase in performance at the global level. To assemble more and more elements into

* Corresponding author. Tel.: +359 66 223 274; fax: +359 66 801 155.
E-mail address: vdzim@tugab.bg (V.D. Zimparov).

0017-9310/$ - see front matter © 2006 Elsevier Ltd. All rights reserved.
doi:10.1016/j.ijheatmasstransfer.2006.05.024

Nomenclature

A	area (m^2)
c_p	specific heat ($J\,kg^{-1}\,K^{-1}$)
D	channel diameter (m)
f	Fanning friction factor
h	heat transfer coefficient ($W\,m^{-2}\,K^{-1}$)
k	thermal conductivity ($W\,m^{-1}\,K^{-1}$)
L	length (m)
M	dimensionless mass flow rate, $M = \dot{m}c_p/(\pi kNuA^{1/2})$
$\dot{m}$	mass flow rate ($kg\,s^{-1}$)
N_s	entropy generation ratio, $N_s = T\dot{S}_{gen}/q$
Nu	Nusselt number, $Nu = h_iD_i/k$
n	number of pairing levels
n_0	number of central ducts
P	pressure (Pa)
q	heat flow (W)
$\tilde{q}$	dimensionless heat flow , $\tilde{q} = q/(\pi kNuA^{1/2}T)$
r	radius (m)
$\dot{S}_{gen}$	entropy generation rate ($W\,K^{-1}$)
$\widetilde{S}_{gen}$	entropy generation number, $\widetilde{S}_{gen} = \dot{S}_{gen}/(\pi kNuA^{1/2})$
s	specific entropy ($J\,kg^{-1}\,K^{-1}$)
T	temperature (K)
T_0	fluid flow temperature (K)
ΔT	temperature difference (K)
u_m	mean fluid flow velocity ($m\,s^{-1}$)
V	volume (m^3)
v	specific volume ($m^3\,kg^{-1}$)
$\dot{W}$	pumping power (W), $\dot{W} = \dot{m}\Delta P/\rho$
$\widetilde{W}$	dimensionless pumping power, $\widetilde{W} = \dot{W}V^2/[(kNu/c_p)^2(v/\rho)A^{5/2})]$

Greek symbols

ϑ	temperature difference
v	kinematic viscosity ($m^2\,s^{-1}$)
ρ	density ($kg\,m^{-3}$)
τ	$\Delta T/T$

Subscripts

i	inlet or channel rank
m	mean
n	number of construction levels
out	outlet

complex structures, and to optimize (with global objective and space constraints) each connection means to *construct*.

Improvement in the global thermodynamic performance of a system means the decrease in the irreversibility (or entropy generation, exergy destruction) that characterizes all the components and processes of the system. An engineering flow system owes its irreversibility to several mechanisms, most notably the flow of heat, fluid and electric current due to driving potentials, and against finite resistances. The entropy generated by each current is proportional to the product of the current times the driving potential, i.e. proportional to the resistance overcome by the current. In simple terms, the entire effort to optimized thermodynamically the greater system rests on the ability to minimize all internal flow resistances, together. Because of constraints, the resistances compete against each other.

The route to improvements in global performance is by *balancing* the reductions in the competing resistances. Thermodynamically, this amounts to spreading the entropy generation rate through the system in an optimal way, so that the total irreversibility is reduced. Optimal spreading of imperfection is achieved by properly sizing, shaping and positioning the components. In the end, the geometry structure of the system – its architecture – emerges as a result of global thermodynamic optimization.

Tree-shaped flows have been studied extensively recently [11–19]. Bejan [20], and da Silva et al. [21] proposed to use dendritic flow architecture in the conceptual design of two-stream heat exchangers. This is a new direction for the development of the heat exchanger architecture. The ultimate goal is to determine flow architectures that reach *simultaneously* two objectives: (i) minimal global fluid resistance (or pumping power), and (ii) minimal thermal resistance. When the architecture is optimized for (i), the result is a dendritic structure in which every geometric feature is uniquely determined. The corresponding thermal resistance decreases as the total mass flow rate and pumping power increase. When the objective is (ii), the optimal architecture has radial ducts, not dendrites. The corresponding fluid-flow resistance increases as the flow rate increases and the global thermal resistance decreases.

In this paper, we continue to develop the idea of a new way of approaching the geometric optimization of tree-shaped paths for fluid flow, as the temperature of the channel wall is fixed. The objective is to determine flow architectures that reach simultaneously two objectives: (i) minimal global entropy generated, and (ii) maximum heat flow density. We consider simple building blocks consisting of a few streams that serve as tributaries or branches in a constrained space. A larger stream with two branches (or two tributaries) forms a construct shaped as T or Y. We also show that by putting together the optimized constructs it is possible to reconstruct features of the much more complicated tree structures optimized so far. Next, we show a performance evaluation criterion for evaluation of the performance of new tree-shaped flow geometries through comparison of the entropy generated in the system with the heat transfer performance achieved.

2. Problem formulation

In order to calculate the entropy generation, we consider an axially uniform duct of circular cross-section with $T_w = \text{constant}$ on its surface. An incompressible viscous fluid with mass flow rate $\dot{m}_i$ and inlet temperature T_i enters the channel with length L_i. The flow is laminar and fully developed (Hagen–Poiseuille). Consider the energy balance of the control volume of length dx

$$h\vartheta\pi D\,dx = -\rho c_p u_m \frac{\pi D^2}{4}\,d\vartheta. \tag{1a}$$

Integrating Eq. (1a) yields

$$\vartheta(x) = \vartheta_i \exp\left(-\frac{\pi kNu}{\dot{m}c_p}x\right), \tag{1b}$$

where $\vartheta_i = T_w - T_i$ is the initial temperature difference. Considering an entropy balance in the same control volume, the rate of entropy generation is

$$d\dot{S}_{gen} + \frac{dq}{T_w} = \dot{m}\,ds. \tag{2a}$$

Assuming the fluid to be an ideal gas or incompressible fluid, and using the thermodynamic relation $T\,ds = c_p dT - v\,dP$ and $q = \dot{m}c_p\,dT$, Eq. (2a) can be written as

$$\frac{d\dot{S}_{gen}}{dx} = \dot{m}c_p\frac{T_w - T}{TT_w}\frac{dT}{dx} + \frac{\dot{m}}{\rho T}\left(-\frac{dP}{dx}\right). \tag{3a}$$

Substituting the values $T_w = T(x) + \Delta T(x)$ and $\tau = \Delta T/T$

$$\frac{d\dot{S}_{gen}}{dx} = \dot{m}c_p\frac{dT}{dx}\frac{\Delta T}{T^2(1+\tau)} + \frac{\dot{m}}{\rho T}\left(-\frac{dP}{dx}\right). \tag{3b}$$

Assuming that $\tau \ll 1$, Eq. (3b) becomes

$$\frac{d\dot{S}_{gen}}{dx} = \dot{m}c_p\frac{\Delta T}{T^2}\frac{dT}{dx} + \frac{\dot{m}}{\rho T}\left(-\frac{dP}{dx}\right), \tag{4}$$

where $T(x) = T_w - \vartheta_i \exp\left(-\frac{\pi kNu}{\dot{m}c_p}x\right)$, $\Delta T = T_w - T(x) = \vartheta_i \exp\left(-\frac{\pi kNu}{\dot{m}c_p}x\right)$ and $\frac{dT}{dx} = \frac{\pi kNu}{\dot{m}c_p}\vartheta_i \exp\left(-\frac{\pi kNu}{\dot{m}c_p}x\right)$. Integrating Eq. (4) along the length of the ith channel

$$\dot{S}_{gen,i} = \frac{q_i\Delta T_{min}}{T_{in}T_{out}} + \frac{32\dot{m}_i^3 f_i L_i}{\rho^2\pi^2 D_i^5 T_w} = \frac{q_i\Delta T_{min,i}}{T_0^2} + \frac{128\nu\dot{m}_i^2 L_i}{\rho\pi T_w D_i^4}. \tag{5}$$

In Eq. (5), $\Delta T_{min,i} = T_w - T_{out,i}$, $q_i = \pi kNuL_i\Delta T_{m,i}$, $f_i = 16/Re_i = 4\pi\rho\nu D_i/\dot{m}_i$, and we assume that $T_{in}T_{out} \cong T_{in}^2 \cong T_{out}^2 = T_0^2$ (T_0 is the fluid flow temperature. It can be T_{in}, T_{out} or T_{av} (average)). For each channel, the mean temperature difference $\Delta T_{m,i}$ is defined as

$$\begin{aligned}\Delta T_{m,i} &= \frac{1}{L_i}\int_0^{L_i}\Delta T_i dx \\ &= \Delta T_{max,i}\frac{\dot{m}_i c_p}{\pi kNuL_i}\left[1 - \exp\left(-\frac{\pi kNuL_i}{\dot{m}_i c_p}\right)\right] \\ &= \frac{\Delta T_{max,i}}{N_i}[1 - \exp(-N_i)],\end{aligned} \tag{6}$$

where $N_i = \frac{\pi kNuL_i}{\dot{m}_i c_p}$ is the local number of heat transfer units, and ΔT_i is defined from Eq. (4),

$$\begin{aligned}\Delta T_i &= T_w - T_i(x) = \Delta T_{max,i}\exp\left(-\frac{\pi kNu}{\dot{m}_i c_p}x\right) \\ &= \Delta T_{max,i}\exp\left(-N_i\frac{x}{L_i}\right).\end{aligned} \tag{7}$$

The maximal $\Delta T_{max,i}$ and minimal $\Delta T_{min,i}$ temperature differences can be obtained from Eq. (7) at $x = 0$, and $x = L_i$, respectively,

$$\begin{aligned}\Delta T_{min,i} &= \Delta T_{max,i+1} = \Delta T_{max,i}\exp\left(-\frac{\pi kNu}{\dot{m}_i c_p}L_i\right) \\ &= \Delta T_{max,i}\exp(-N_i).\end{aligned} \tag{8}$$

For tree-shaped heat exchanger, the overall entropy generated is

$$\begin{aligned}\dot{S}_{gen} &= \sum_{i=0}^{n} n_i\dot{S}_{gen,i} \\ &= \frac{1}{T_0^2}\sum_{i=0}^{n} n_i q_i\Delta T_{min,i} + \frac{128\nu}{\rho\pi T_w}\sum_{i=0}^{n} n_i\dot{m}_i^2\frac{L_i}{D_i^4},\end{aligned} \tag{9}$$

where

$$\begin{aligned}q_i &= \pi kNuL_i\Delta T_{m,i} = \dot{m}_i c_p\Delta T_x^i \\ &= \dot{m}_i c_p\Delta T_{max,i}\left[1 - \exp\left(-\frac{\pi kNu}{\dot{m}_i c_p}L_i\right)\right] \\ &= \dot{m}_i c_p\Delta T_{max,i}[1 - \exp(-N_i)].\end{aligned} \tag{10}$$

The maximal temperature difference in each channel, $\Delta T_{max,i}$, is defined as follows:

$$\begin{aligned}&\Delta T_{max,i} = \Delta T_{max} = T_w - T_0, \quad i = 0 \\ &\Delta T_{max,i} = \Delta T_{max}\exp\left(-\sum_{k=0}^{i-1} N_k\right), \quad i = 1,2,\ldots,n.\end{aligned} \tag{11}$$

Thus, the minimal temperature difference in each channel, $\Delta T_{min,i}$, Eq. (8), becomes

$$\Delta T_{min,i} = \Delta T_{max}\exp\left(-\sum_{k=0}^{i} N_k\right), \quad i = 0,1,\ldots,n. \tag{12}$$

Eq. (9) can be presented in dimensionless form as

$$\begin{aligned}\frac{\dot{S}_{gen}}{\pi kNuA^{1/2}} &\equiv \widetilde{S}_{gen} \\ &= \frac{1}{\pi kNuA^{1/2}T_0^2}\sum_{i=0}^{n} n_i q_i\Delta T_{min,i} \\ &\quad + \frac{128\nu}{\rho\pi^2 kNuA^{1/2}T_w}\sum_{i=0}^{n} n_i\dot{m}_i^2\frac{L_i}{D_i^4}.\end{aligned} \tag{13}$$

The overall enthalpy change is $q = \dot{m}c_p\Delta T_x$, where ΔT_x is the overall longitudinal temperature excursion

$$\Delta T_x = \sum_{i=0}^{n}\Delta T_{x,i} = \sum_{i=0}^{n}\Delta T_{max,i}[1 - \exp(-N_i)]. \tag{14}$$

The heat flow can also be obtained as

$$q = \sum_{i=0}^{n} n_i q_i = \sum_{i=0}^{n} n_i \dot{m}_i c_p \Delta T_{\max,i}[1 - \exp(-N_i)] = n_0 \dot{m}_0 c_p \Delta T_{\max}[1 - \exp(-N_0)] + c_p \Delta T_{\max} \sum_{i=1}^{n} n_i \dot{m}_i \exp\left(-\sum_{k=0}^{i-1} N_k\right)[1 - \exp(-N_i)]. \quad (15)$$

3. Laminar flow in a T-shaped assembly of tubes – first construct

Consider first the case of incompressible flow through the T-shaped structure, Fig. 1, for which $n = 1$, $n_i = 2^{n-i} = 2^{1-i}$, $\dot{m}_i = 2^i \dot{m}_0$, $\dot{m} = 2^n \dot{m}_0 = 2\dot{m}_0$. The flow is laminar and fully developed (Hagen–Poiseuille). The total volume occupied by the tubes is fixed,

$$V = \sum n_i \frac{\pi}{4} D_i^2 L_i = \frac{\pi}{4}(2D_0^2 L_0 + D_1^2 L_1) = \text{const.} \quad (16)$$

Fixed is also the total space occupied by the planar structure,

$$A = (4L_0)(2L_1) = 8L_0 L_1 = \text{const.} \quad (17)$$

The objective is to minimize the entropy generation, $\widetilde{S}_{\text{gen}}$, Eq. (13). For this particular case,

$$\sum_{i=0}^{n} n_i q_i \Delta T_{\min,i} = \sum_{i=0}^{1} 2^{1-i} q_i \Delta T_{\min,i} = 2q_0 \Delta T_{\min,0} + q_1 \Delta T_{\min,1} = \dot{m} c_p \Delta T_{\max}^2 \exp\left(-\frac{2^{-1/2}}{M\widetilde{L}^{1/2}}\right) \times \left\{\left[1 - \exp\left(-\frac{2^{-1/2}}{M\widetilde{L}^{1/2}}\right)\right] + \exp\left(-\frac{2+\widetilde{L}}{2^{3/2}M\widetilde{L}^{1/2}}\right) \times \left[1 - \exp\left(-\frac{2^{-3/2}\widetilde{L}^{1/2}}{M}\right)\right]\right\}$$

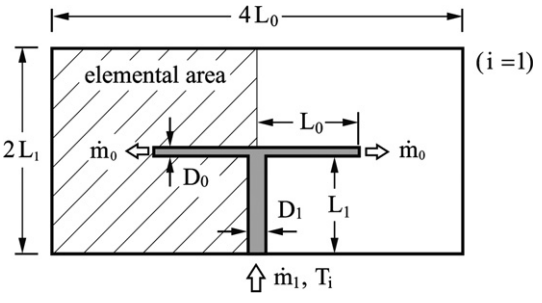

Fig. 1. T-shaped assembly of round tubes.

and

$$\sum_{i=0}^{n} n_i \dot{m}_i^2 \frac{L_i}{D_i^4} = \dot{m}^2\left(\frac{L_0}{2D_0^4} + \frac{L_1}{D_1^4}\right) = \frac{\dot{m}^2 L_0}{2D_0^4}\left(1 + \frac{2\widetilde{L}}{\widetilde{D}^4}\right),$$

where $\widetilde{L} = L_1/L_0$, $L_0 = 2^{-3/2}A^{1/2}\widetilde{L}^{-1/2}$, and $\widetilde{D} = D_1/D_0$. The first term in Eq. (13) does not depend on $\widetilde{D}$ and the optimization of the entropy generation, Eq. (13), with respect to $\widetilde{D}$ follows the same procedure as that developed by Bejan et al. [13]. It gives the well known result of $\widetilde{D} = 2^{1/3}$. Thus,

$$\sum_{i=0}^{n} n_i \dot{m}_i^2 \frac{L_i}{D_i^4} = \frac{\dot{m}^2 L_0}{2D_0^4}(1 + 2^{-1/3}\widetilde{L}) = \frac{\dot{m}^2 \pi^2 A^{3/2}}{128 V^2 2^{1/2}} \frac{(1 + 2^{-1/3}\widetilde{L})^3}{\widetilde{L}^{3/2}}.$$

Accordingly, the first term of Eq. (13) becomes

$$\widetilde{S}_{\text{gen},\Delta T} = \frac{1}{\pi k Nu A^{1/2} T_0^2} \sum_{i=0}^{n} n_i q_i \Delta T_{\min,i} = \frac{\dot{m} c_p \Delta T_{\max}^2}{\pi k Nu A^{1/2} T_0^2} \exp\left(-\frac{2^{-1/2}}{M\widetilde{L}^{1/2}}\right) \times \left\{\left[1 - \exp\left(-\frac{2^{-1/2}}{M\widetilde{L}^{1/2}}\right)\right] + \exp\left(-\frac{2+\widetilde{L}}{2^{3/2}M\widetilde{L}^{1/2}}\right) \times \left[1 - \exp\left(-\frac{2^{-3/2}\widetilde{L}^{1/2}}{M}\right)\right]\right\}, \quad (18)$$

whereas the second term yields

$$\widetilde{S}_{\text{gen},\Delta P} = \frac{128\nu}{\rho\pi^2 k Nu A^{1/2} T_{\text{w}}} \sum_{i=0}^{n} n_i \dot{m}_i^2 \frac{L_i}{D_i^4} = \frac{\nu k Nu}{\rho c_p^2 T_{\text{w}}} \frac{\pi^2 A^2}{V^2 2^{1/2}} M^2 \frac{(1 + 2^{-1/3}\widetilde{L})^3}{\widetilde{L}^{3/2}}. \quad (19)$$

Finally, Eq. (13) can be presented in the form

$$\widetilde{S}_{\text{gen}} = M(T^* - 1)^2 \exp\left(-\frac{2^{-1/2}}{M\widetilde{L}^{1/2}}\right) \times \left\{\left[1 - \exp\left(-\frac{2^{-1/2}}{M\widetilde{L}^{1/2}}\right)\right] + \exp\left(-\frac{2+\widetilde{L}}{2^{3/2}M\widetilde{L}^{1/2}}\right) \times \left[1 - \exp\left(-\frac{2^{-3/2}\widetilde{L}^{1/2}}{M}\right)\right]\right\} + B_1 M^2 \frac{(1 + 2^{-1/3}\widetilde{L})^3}{\widetilde{L}^{3/2}}, \quad (20)$$

where

$$B_1 = \frac{\pi^2 \nu k Nu A^2}{2^{1/2}\rho c_p^2 V^2 T_{\text{w}}}, \quad \text{and} \quad T^* = T_{\text{w}}/T_0. \quad (21)$$

Eq. (20) can also be presented in the form

$$\widetilde{S}_{\text{gen}} = M(T^*-1)^2 \times \left[\exp\left(-\frac{2^{-1/2}}{M\widetilde{L}^{1/2}}\right) \times \left\{\left[1-\exp\left(-\frac{2^{-1/2}}{M\widetilde{L}^{1/2}}\right)\right] + \exp\left(-\frac{2+\widetilde{L}}{2^{3/2}M\widetilde{L}^{1/2}}\right) \times \left[1-\exp\left(-\frac{2^{-3/2}\widetilde{L}^{1/2}}{M}\right)\right]\right\} + \frac{B_1 M}{(T^*-1)^2}\frac{(1+2^{-1/3}\widetilde{L})^3}{\widetilde{L}^{3/2}}\right]. \quad (22)$$

The limiting cases are:

(i) $T^* = 1$ (isothermal condition), when

$$\widetilde{S}_{\text{gen}} = B_1 M^2 \frac{(1+2^{-1/3}\widetilde{L})^3}{\widetilde{L}^{3/2}} \quad (23)$$

and the minimization of $\widetilde{S}_{\text{gen}}$ ($\mathrm{d}\widetilde{S}_{\text{gen}}/\mathrm{d}\widetilde{L} = 0$) subject to constraints A and V yields the ratio $\widetilde{L}_{\text{opt}} = 2^{1/3}$. The same result was obtained in Ref. [13] from the principle of minimum global flow resistance.

(ii) $T^* > 1$, and $B^* = \frac{B_1 M}{(T^*-1)^2} \gg 1$, when

$$\widetilde{S}_{\text{gen}} = B_1 M^2 \frac{(1+2^{-1/3}\widetilde{L})^3}{\widetilde{L}^{3/2}}.$$

The result is the same as in case (i).

(iii) $T^* > 1$, and $B^* = \frac{B_1 M}{(T^*-1)^2} \ll 1$, when

$$\widetilde{S}_{\text{gen}} = M(T^*-1)^2 \exp\left(-\frac{2^{-1/2}}{M\widetilde{L}^{1/2}}\right) \times \left\{\left[1-\exp\left(-\frac{2^{-1/2}}{M\widetilde{L}^{1/2}}\right)\right] + \exp\left(-\frac{2+\widetilde{L}}{2^{3/2}M\widetilde{L}^{1/2}}\right)\left[1-\exp\left(-\frac{2^{-3/2}\widetilde{L}^{1/2}}{M}\right)\right]\right\} \quad (24)$$

and the result for $\widetilde{L}_{\text{opt}}$ is again $\widetilde{L}_{\text{opt}} = 2^{1/3}$. In the intermediate range $10^{-2} < B^* < 10^3$, the results of $\widetilde{L}_{\text{opt}}$, Table 1, show very small variations around $\widetilde{L}_{\text{opt}} = 2^{1/3}$. It can be concluded that the optimal length ratio is $\widetilde{L}_{\text{opt}} = 2^{1/3}$ despite the value of B^*. This result confirms again the result obtained in Ref. [13] from the principle of minimum global flow resistance.

Table 1
The variation of L_{opt} with B^*

B^*	$\widetilde{L}_{\text{opt}}$
0.01	1.25992105
0.1	1.243493877
1	1.247552317
10	1.260169892
100	1.259924406
1000	1.25992105

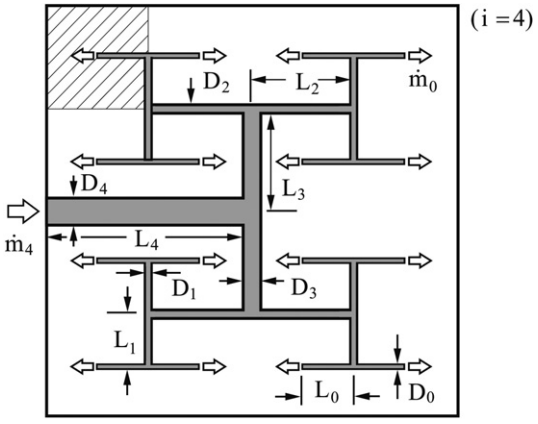

Fig. 2. Flow of tree-shaped streams distributed over a square area.

Fig. 2 presents tree-shaped streams distributed over a square area. This configuration was designed from the principle of minimal global flow resistance. The numbers and flow rates are ordered as

$$n_i = 2^{n-i}, \quad \dot{m}_i = 2^i \dot{m}_0 \qquad (i = 0, 1, \ldots, n). \quad (25)$$

The lengths are obeyed the length-doubling rule by writing approximately [17] $L_i = 2^{i/2} L_0$, and

$$L_0 = \frac{A^{1/2}}{2^{(n+2)/2}}, \quad D_0 = \frac{2^{(6-n)/4} V^{1/2}}{\pi^{1/2} A^{1/4} S_1^{1/2}}. \quad (26)$$

For this design configuration,

$$q = \dot{m} c_p \Delta T_{\max}\left\{\left[1-\exp\left(-\frac{2^{(n-2)/2}}{M}\right)\right] + \sum_{i=1}^{n} \exp\left(-\sum_{k=0}^{i-1}\frac{2^{(n-k-2)/2}}{M}\right)\left[1-\exp\left(-\frac{2^{(n-i-2)/2}}{M}\right)\right]\right\} \quad (27)$$

or

$$\tilde{q} = \frac{q}{\pi k Nu A^{1/2} T_0} = M(T^*-1)\left\{\left[1-\exp\left(-\frac{2^{(n-2)/2}}{M}\right)\right] + S_2\right\}, \quad (28)$$

$$\sum_{i=0}^{n} n_i q_i \Delta T_{\min,i} = \dot{m} c_p \Delta T_{\max}^2 \left\{\exp\left(-\frac{2^{(n-2)/2}}{M}\right) \times \left[1-\exp\left(-\frac{2^{(n-2)/2}}{M}\right)\right] + S_3\right\} \quad (29)$$

and the entropy generation number, Eq. (13), yields

$$\widetilde{S}_{\text{gen}} = M(T^*-1)^2\left\{\exp\left(-\frac{2^{(n-2)/2}}{M}\right) \times \left[1-\exp\left(-\frac{2^{(n-2)/2}}{M}\right)\right] + S_3\right\} + M^2 B_2 \frac{S_1^3}{2^{n/2}}, \quad (30)$$

where

$$S_1 = \sum_{i=0}^{n} 2^{i/6} = \frac{2^{(n+1)/6} - 1}{2^{1/6} - 1}, \tag{31}$$

$$S_2 = \sum_{i=1}^{n} \exp\left(-\sum_{k=0}^{i-1} \frac{2^{(n-k-2)/2}}{M}\right)\left[1 - \exp\left(-\frac{2^{(n-i-2)/2}}{M}\right)\right], \tag{32}$$

$$S_3 = \sum_{i=1}^{n} \left[\exp\left(-\sum_{k=0}^{i-1} \frac{2^{(n-k-2)/2}}{M}\right)\right]^2 \exp\left(-\frac{2^{(n-i-2)/2}}{M}\right) \times \left[1 - \exp\left(-\frac{2^{(n-i-2)/2}}{M}\right)\right] \tag{33}$$

and $B_2 = \frac{\nu k N u \pi^2 A^2}{\rho c_p^2 T_w V^2}$. Eq. (30) gives the variation of $\widetilde{S}_{gen}$ with M and n at fixed B_2 and T^*, and is to be used in the case of specified mass flow rate, M. Fig. 3 shows the variation of entropy generation number $\widetilde{S}_{gen}$ with mass flow rate M and number of channels, n, at fixed B_2 and T^*. As expected, the entropy generation $\widetilde{S}_{gen}$ increases with the mass flow rate M and with the complexity n. A secondary effect is the appearance of diminishing returns as n increases. Additionally, it should be noted that the variation of $\widetilde{S}_{gen}$ does not depend on the value of the parameter T^*.

The performance of the tree-shaped flow geometries can be evaluated through entropy generation ratio N_s which compares the entropy generated in the system with the heat transfer performance achieved. The increase of the number of branches increases the entropy generated in the system. At the same time, however, overall heat flow, Eq. (27), increases as well. To compare the entropy generated in the system with the heat transfer performance achieved in the tree-shape design, we combine Eqs. (28) and (30) in the ratio

$$N_s = \frac{\widetilde{S}_{gen}}{\tilde{q}} \equiv \frac{T_0 \dot{S}_{gen}}{q} = \frac{(T^* - 1)\left\{\exp\left(-\frac{2^{(n-2)/2}}{M}\right)\left[1 - \exp\left(-\frac{2^{(n-2)/2}}{M}\right)\right] + S_3\right\}}{\left\{\left[1 - \exp\left(-\frac{2^{(n-2)/2}}{M}\right)\right] + S_2\right\}} + \frac{S_1^3}{2^{n/2}(T^* - 1)} \frac{B_2 M}{\left\{\left[1 - \exp\left(-\frac{2^{(n-2)/2}}{M}\right)\right] + S_2\right\}}. \tag{34}$$

Eq. (34) gives the variation of N_s with M and n at fixed B_2 and T^*, and is to be used in the case of specified mass flow rate, M. Fig. 4 shows the variation of entropy generation ratio N_s with mass flow rate M and number of channels n, at fixed B_2 and T^*. As seen in Fig. 4 N_s increases with M at two different rates, and the transition between these two limits happens around $M \sim 50$. For small mass flow rates, $M < 1$, the entropy generation number increases with M at a smaller rate when compared with the increasing rate at large mass flow rate regimes, $M > 10^2$. Additionally, Fig. 4 shows the detrimental effect of the complexity n on the entropy generation ratio N_s throughout the whole range of mass flow rate considered, $10^{-3} < M < 10^3$, with the appearance of diminishing returns as n increase. Similarly to the effect of M on N_s, the complexity n also acts differently on N_s depending on the mass flow rate considered. For values of $M < 1$, the diminishing return rate is much smaller than the large mass flow rate limit, $M > 10^2$, where n has basically no effect on the entropy generations ratio if $n > 3$.

In the case of fixed pumping power, $\widetilde{W} = \text{const}$, Eq. (34) can be transformed using the relationship [21]:

$$M = \frac{2^{n/4}}{\pi^{3/2} S_1^{3/2}} \widetilde{W}^{1/2}. \tag{35}$$

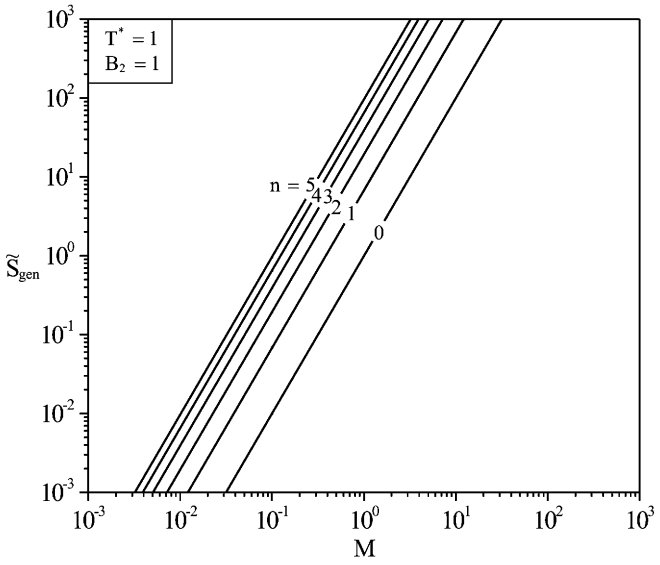

Fig. 3. Effect of the mass flow rate M and complexity n on the dimensionless entropy generation $\widetilde{S}_{gen}$ for a tree-shaped structure distributed over a square area.

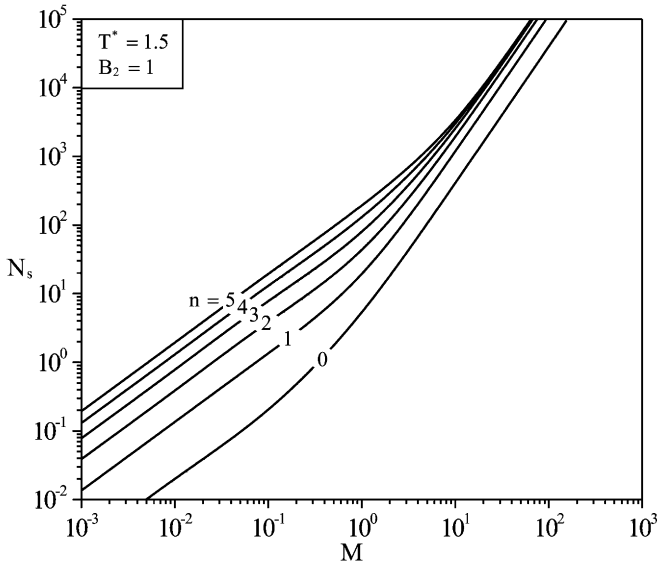

Fig. 4. Effect of the mass flow rate M and complexity n on the entropy generation ratio N_s for a tree-shaped structure distributed over a square area.

Fig. 5 shows the variation of entropy generation ratio N_s with pumping power $\widetilde{W}$ and number of channels n, at fixed B_2 and T^*. On the contrary of Fig. 4 where N_s increases unconditionally with M and n, here, higher complexity levels are proven to be profitable at certain values of $\widetilde{W}$. This behaviour permits an envelope curve of minimum entropy generation number for any pumping power available to be drawn. This means that when $\widetilde{W}$ is constrained, the simplest configuration (i.e. smaller n) is not necessarily the best design as shown previously, Fig. 4.

Fig. 6 shows the envelope curves of minimal N_s for three different values of T^*. The vertical dashed lines indicate the optimal complexity for each one of the three T^* envelope curves. It is important to notice that range to validity of a given optimal complexity shifts slightly to the left as T^* increases. Also, the effectiveness of the design increases with the increase of the parameter T^*.

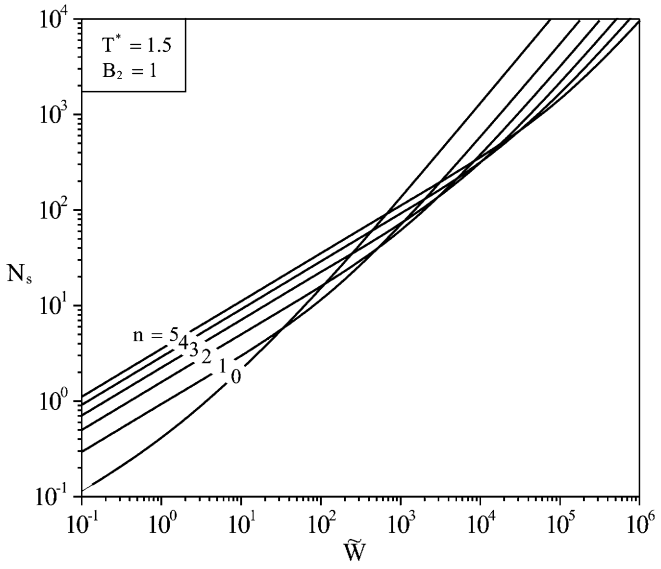

Fig. 5. Effect of the dimensionless pumping power $\widetilde{W}$ and complexity n on the entropy generation ratio N_s for a tree-shaped structure distributed over a square area.

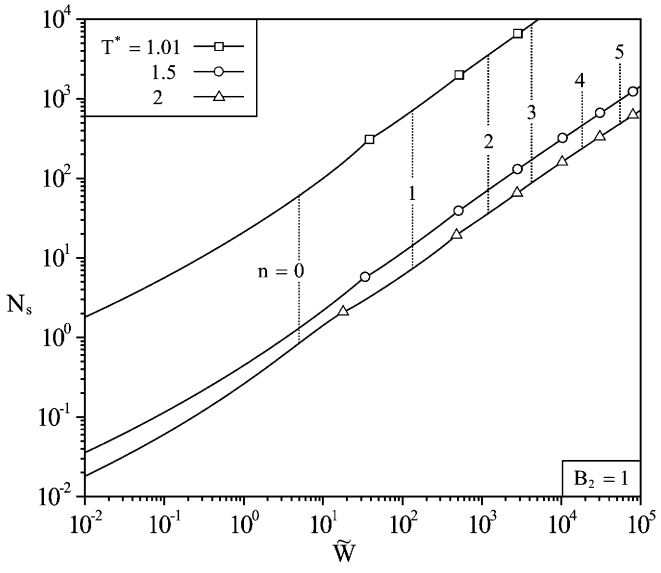

Fig. 6. Envelope curves of minimal entropy generation ratio (N_s) for a tree-shaped structure distributed over a square area ($\Delta T^* = 1.01$, 1.5 and 2).

4. Y-shaped assembly in a circle area

The next problem is Y-shaped construct of two L_0, and one L_1 tubes occupying the fixed area A of the circle sector of angle α, Fig. 7. The geometry of the Y-shaped construct depends on the radial position of the node (i.e. the length L_1), or the angle β. Both L_0 and L_1 vary with β, when r is fixed:

$$L_0 = r\frac{\sin\left(\frac{\alpha}{4}\right)}{\sin\beta} = r\frac{\sin\left(\frac{\pi}{2n_0}\right)}{\sin\beta}, \tag{36}$$

$$L_1 = r\cos\left(\frac{\alpha}{4}\right) - r\frac{\sin\left(\frac{\alpha}{4}\right)}{\tan\beta} = r\cos\left(\frac{\pi}{2n_0}\right) - r\frac{\sin\left(\frac{\pi}{2n_0}\right)}{\tan\beta}, \tag{37}$$

$$\widetilde{L} = L_1/L_0 = \frac{\sin\beta}{\tan\left(\frac{\pi}{2n_0}\right)} - \cos\beta, \tag{38}$$

$\alpha = \frac{2\pi}{n_0}$, $A = \frac{\pi r^2}{n_0}$, and n_0 is the number of tubes leaving the centre. For this case, the quantities in Eq. (13) yield

$$\begin{aligned}
&\sum_{i=0}^{n} n_i q_i \Delta T_{\min,i} \\
&= 2q_0\Delta T_{\min,0} + q_1\Delta T_{\min,1} \\
&= \frac{\dot{m}c_p}{n_0}\Delta T_{\max}^2 \exp\left[-\frac{2n_0}{\pi^{1/2}M}\frac{\sin\left(\frac{\pi}{2n_0}\right)}{\sin\beta}\right] \\
&\quad\times\left(\left\{1-\exp\left[-\frac{2n_0}{\pi^{1/2}M}\frac{\sin\left(\frac{\pi}{2n_0}\right)}{\sin\beta}\right]\right\}\right. \\
&\quad+\left(1-\exp\left\{-\frac{n_0}{\pi^{1/2}M}\left[\cos\left(\frac{\pi}{2n_0}\right)-\frac{\sin\left(\frac{\pi}{2n_0}\right)}{\tan\beta}\right]\right\}\right) \\
&\quad\left.\times\exp\left\{-\frac{n_0}{\pi^{1/2}M}\left[\frac{2\sin\left(\frac{\pi}{2n_0}\right)}{\sin\beta}+\cos\left(\frac{\pi}{2n_0}\right)-\frac{\sin\left(\frac{\pi}{2n_0}\right)}{\tan\beta}\right]\right\}\right)
\end{aligned} \tag{39}$$

and

$$\begin{aligned}
\sum_{i=0}^{n} n_i\dot{m}_i^2\frac{L_i}{D_i^4} &= \frac{\dot{m}^2}{2n_0^2}\frac{\pi^{1/2}A^{3/2}}{4V^2} \\
&\quad\times\frac{\sin^3\left(\frac{\pi}{2n_0}\right)}{\sin^3\beta}\left\{1+2^{-1/3}\left[\frac{\sin\beta}{\tan\left(\frac{\pi}{2n_0}\right)}-\cos\beta\right]\right\}^3.
\end{aligned} \tag{40}$$

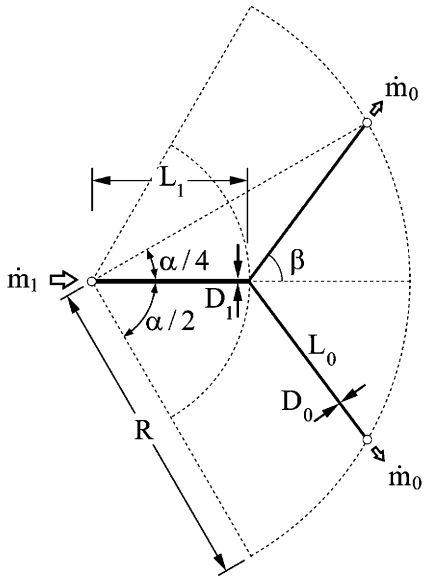

Fig. 7. Sketch of a Y-shaped assembly occupying a fixed area of a circle sector.

Thus, the first term in Eq. (13) becomes

$$\widetilde{S}_{\mathrm{gen},\Delta T} = \frac{M(T^*-1)^2}{n_0}\exp\left[-\frac{2n_0}{\pi^{1/2}M}\frac{\sin\left(\frac{\pi}{2n_0}\right)}{\sin\beta}\right] \times\left(\left\{1-\exp\left[-\frac{2n_0}{\pi^{1/2}M}\frac{\sin\left(\frac{\pi}{2n_0}\right)}{\sin\beta}\right]\right\} +\left(1-\exp\left\{-\frac{n_0}{\pi^{1/2}M}\left[\cos\left(\frac{\pi}{2n_0}\right)-\frac{\sin\left(\frac{\pi}{2n_0}\right)}{\tan\beta}\right]\right\}\right) \times\exp\left\{-\frac{n_0}{\pi^{1/2}M}\left[\frac{2\sin\left(\frac{\pi}{2n_0}\right)}{\sin\beta}+\cos\left(\frac{\pi}{2n_0}\right)-\frac{\sin\left(\frac{\pi}{2n_0}\right)}{\tan\beta}\right]\right\}\right). \tag{41}$$

The second term in Eq. (13) yields

$$\widetilde{S}_{\mathrm{gen},\Delta P} = \frac{B_3M^2}{n_0^2}\frac{\sin^3\left(\frac{\pi}{2n_0}\right)}{\sin^3\beta}\left\{1+2^{-1/3}\left[\frac{\sin\beta}{\tan\left(\frac{\pi}{2n_0}\right)}-\cos\beta\right]\right\}^3, \tag{42}$$

where $B_3=\frac{16\pi^{1/2}\gamma k Nu A^2}{\rho c_p^2 V^2 T_w}$. The limiting cases are:

(i) $T^*=1$ (isothermal condition), when

$$\widetilde{S}_{\mathrm{gen}} = \frac{B_3M^2}{n_0^2}\frac{\sin^3\left(\frac{\pi}{2n_0}\right)}{\sin^3\beta}\left\{1+2^{-1/3}\left[\frac{\sin\beta}{\tan\left(\frac{\pi}{2n_0}\right)}-\cos\beta\right]\right\}^3, \tag{43}$$

For this limiting case, the optimal angle of confluence is $\beta_{\mathrm{opt}}=0.654$ rad(37.47) regardless of n_0, whereas $\widetilde{L}_{\mathrm{opt}}$ depends on n_0: $n_0=3$, $\widetilde{L}_{\mathrm{opt}}=1$; $n_0=5$, $\widetilde{L}_{\mathrm{opt}}=2.165$; $n_0=10$, $\widetilde{L}_{\mathrm{opt}}=4.967$. The same result was obtained in [18] from the principle of minimum global flow resistance.

(ii) $T^*>1$, and $B^*=\frac{B_3M}{n_0(T^*-1)^2}\gg 1$, when

$$\widetilde{S}_{\mathrm{gen}} = \frac{B_3M^2}{n_0^2}\frac{\sin^3\left(\frac{\pi}{2n_0}\right)}{\sin^3\beta}\left\{1+2^{-1/3}\left[\frac{\sin\beta}{\tan\left(\frac{\pi}{2n_0}\right)}-\cos\beta\right]\right\}^3. \tag{44}$$

The result is the same as in case (i).

(iii) $T^*>1$, and $B^*=\frac{B_3M}{n_0(T^*-1)^2}\ll 1$, when

$$\widetilde{S}_{\mathrm{gen}} = \frac{M(T^*-1)^2}{n_0}\exp\left[-\frac{2n_0}{\pi^{1/2}M}\frac{\sin\left(\frac{\pi}{2n_0}\right)}{\sin\beta}\right] \times\left(\left\{1-\exp\left[-\frac{2n_0}{\pi^{1/2}M}\frac{\sin\left(\frac{\pi}{2n_0}\right)}{\sin\beta}\right]\right\} +\left(1-\exp\left\{-\frac{n_0}{\pi^{1/2}M}\left[\cos\left(\frac{\pi}{2n_0}\right)-\frac{\sin\left(\frac{\pi}{2n_0}\right)}{\tan\beta}\right]\right\}\right) \times\exp\left\{-\frac{n_0}{\pi^{1/2}M}\left[\frac{2\sin\left(\frac{\pi}{2n_0}\right)}{\sin\beta} +\cos\left(\frac{\pi}{2n_0}\right)-\frac{\sin\left(\frac{\pi}{2n_0}\right)}{\tan\beta}\right]\right\}\right). \tag{45}$$

For this case there is no β_{opt} and L_{opt}.

When the two terms of entropy generation number $\widetilde{S}_{\mathrm{gen}}$ are comparable the results for β_{opt} and L_{opt} depend on the values of M and n_0. Table 2 shows the results for β_{opt} and L_{opt} for values of $n_0=4$, 5, 6 and 10 in the range $10^{-5}<M<10^5$, for $B_3=1$ and $T^*=1.25$. It is remarkably that for $n_0=5$, the values of $\beta_{\mathrm{opt}}=0.654$ and $L_{\mathrm{opt}}=1.078$ almost do not depend on the values of M. There are no real values of β_{opt} and L_{opt} for values of $n_0\neq 5$.

Disc-shaped tree flow structure was optimized in [15] for minimum overall flow resistance. The numbers and flow rates are ordered as follows:

$$n_i=2^{n-i}n_0,\quad \dot{m}_i=2^{i-n}\frac{\dot{m}}{n_0}\qquad (i=0,1,\ldots,n). \tag{46}$$

The lengths are presented in dimensionless form as

$$\widehat{L}_i=L_i/R, \tag{47}$$

Table 2
The variation of β_{opt} and L_{opt} for $B_3 = 1$ and $T^* = 1.25$

M	$n_0 = 4$		$n_0 = 5$		$n_0 = 6$		$n_0 = 10$	
	β_{opt}	L_{opt}	β_{opt}	L_{opt}	β_{opt}	L_{opt}	β_{opt}	L_{opt}
10^{-5}			0.653927	1.07848				
10^{-4}			0.653927	1.07848				
10^{-3}			0.653927	1.07848				
10^{-2}			0.653927	1.07848				
10^{-1}			0.653927	1.07848				
1			0.652626	1.07451				
10^{1}			0.653933	1.07850				
10^{2}	1.04448	1.58512	0.653929	1.07848	1.051505	2.74379	1.06614	5.04318
10^{3}	1.04696	1.59027	0.653928	1.07848	1.047625	2.73322	1.04896	4.97494
10^{4}	1.04717	1.59072	0.653928	1.07848	1.047240	2.73217	1.04737	4.96857
10^{5}	1.04720	1.59076	0.653928	1.07848	1.047202	2.73206	1.04722	4.96794

where

$$R = \frac{A^{1/2}}{\pi^{1/2}}, \quad D_0 = \frac{V^{1/2} S_4^{-1/2}}{\pi^{1/4} A^{1/4} n_0^{1/2} 2^{(n-2)/2}},$$

and

$$S_4 = \sum_{i=0}^{n} 2^{-i/3} \widehat{L}_i.$$

For this design, the entropy generation number, Eq. (13), yields

$$\widetilde{S}_{gen} = M(T^* - 1)^2 \left\{ \exp\left(-\frac{n_0 2^n}{\pi^{1/2} M} \widehat{L}_0 \right) \times \left[1 - \exp\left(-\frac{n_0 2^n}{\pi^{1/2} M} \widehat{L}_0 \right) \right] + S_5 \right\} + B_4 n_0 2^n S_4^3 M^2, \tag{48}$$

where

$$S_5 = \sum_{i=1}^{n} \left\{ \left[1 - \exp\left(-\frac{n_0 2^n}{\pi^{1/2} M} \frac{\widehat{L}_i}{2^i} \right) \right] \exp\left(-\frac{n_0 2^n}{\pi^{1/2} M} \sum_{k=0}^{i} 2^{-k} \widehat{L}_k \right) \right\} \tag{49}$$

and $B_4 = \frac{8\pi^{1/2} \nu k Nu A^2}{\rho c_p^2 T_w V^2}$. The overall heat flow is

$$q = \dot{m} c_p \Delta T_{max} \left\{ 2^{-n} \left[1 - \exp\left(-\frac{n_0 2^n}{\pi^{1/2} M} \widehat{L}_0 \right) \right] + S_6 \right\} \tag{50}$$

or

$$\tilde{q} = M(T^* - 1) \left\{ 2^{-n} \left[1 - \exp\left(-\frac{n_0 2^n}{\pi^{1/2} M} \widehat{L}_0 \right) \right] + S_6 \right\}, \tag{51}$$

where

$$S_6 = \sum_{i=1}^{n} \left\{ \left[1 - \exp\left(-\frac{n_0 2^n}{\pi^{1/2} M} \frac{\widehat{L}_i}{2^i} \right) \right] \exp\left(-\sum_{k=0}^{i-1} \frac{n_0 2^n}{\pi^{1/2} M} \frac{\widehat{L}_k}{2^k} \right) \right\}. \tag{52}$$

Eq. (48) presents the variation of $\widetilde{S}_{gen}$ with M and n, at fixed n_0, B_4, and T^*. Fig. 8 shows the variation of $\widetilde{S}_{gen}$ with M at $B_4 = 1$, $n_0 = 3$ and $T^* = 1.25$. Similar to the behaviour of the square tree-shaped design presented in Fig. 3, $\widetilde{S}_{gen}$ increases with M for the disc-shaped design,

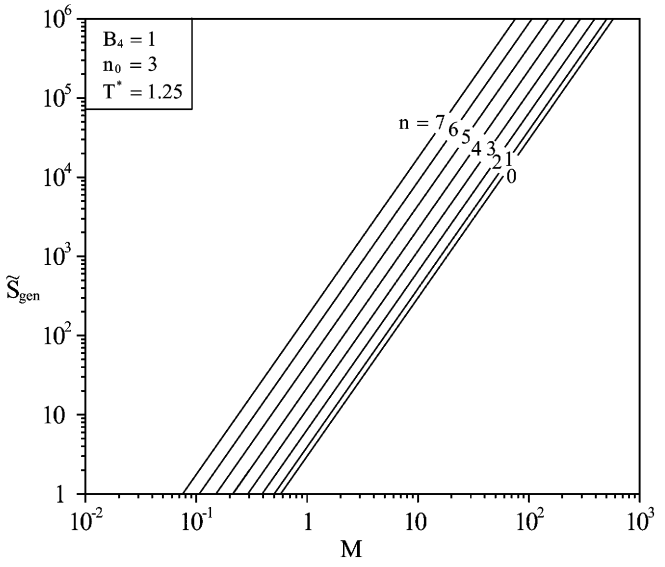

Fig. 8. Effect of the mass flow rate M and complexity n on the dimensionless entropy generation $\widetilde{S}_{gen}$ for the dendritic structure of Fig. 7.

however, no diminishing returns are found as n increases. Actually, the step taken by the each $\widetilde{S}_{gen}$ curve increases slightly with n.

To compare the entropy generated in the system with the heat transfer performance achieved in the tree-shape design, we combine Eqs. (48) and (51) in the ratio

$$N_s = \frac{\widetilde{S}_{gen}}{\tilde{q}} \equiv \frac{T_0 \dot{S}_{gen}}{q} = (T^* - 1) \frac{\left\{ \exp\left(-\frac{n_0 2^n}{\pi^{1/2} M} \widehat{L}_0 \right) \left[1 - \exp\left(-\frac{n_0 2^n}{\pi^{1/2} M} \widehat{L}_0 \right) \right] + S_5 \right\}}{\left\{ 2^{-n} \left[1 - \exp\left(-\frac{n_0 2^n}{\pi^{1/2} M} \widehat{L}_0 \right) \right] + S_6 \right\}} + B_4 \frac{n_0 2^n S_4^3 M}{(T^* - 1) \left\{ 2^{-n} \left[1 - \exp\left(-\frac{n_0 2^n}{\pi^{1/2} M} \widehat{L}_0 \right) \right] + S_6 \right\}}. \tag{53}$$

Eq. (53) gives the variation of N_s with M and n, the case of fixed mass flow rate, $M = \text{const}$, at fixed n_0, B_4, and T^*. Fig. 9 shows the variation of entropy generation ratio N_s with mass flow rate M and number of channels n, at $B_4 = 1$, $n_0 = 3$ and $T^* = 1.25$. It is obvious that for small

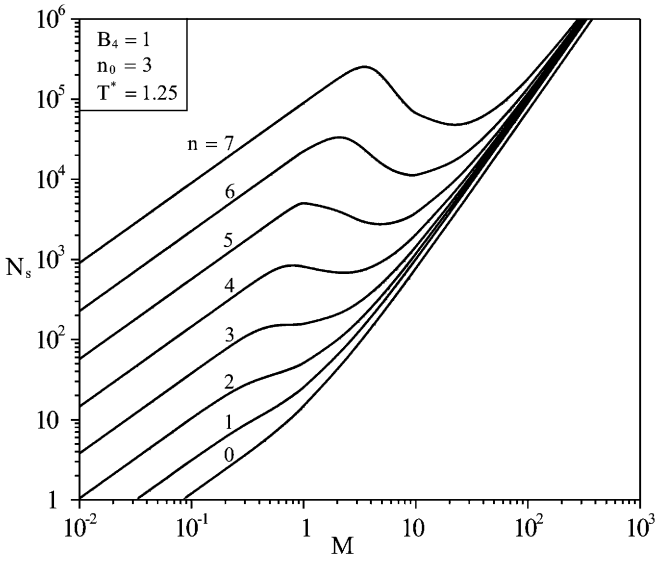

Fig. 9. Effect of the mass flow rate M and complexity n on the entropy generation ratio N_s for the dendritic structure of Fig. 7.

mass flow rates, $M < 1$, the entropy generation number increases with the increase of complexity (number of channels). For higher mass flow rates, $M > 10^2$, the influence of the number of channels on the entropy generation number disappears and no diminishing returns can be identified as n increases for the range of $10^{-2} < M < 10^3$.

In the case of fixed pumping power, $\widetilde{W} = \text{const}$, Eqs. (48) and (51) are to be used with relation

$$M = \frac{\widetilde{W}^{1/2}}{\pi^{3/4} 2^{(n+3)/2} n_0^{1/2} S_4^{3/2}}. \tag{54}$$

Fig. 10 shows the variation of entropy generation ratio N_s with pumping power $\widetilde{W}$ and number of channels n, at

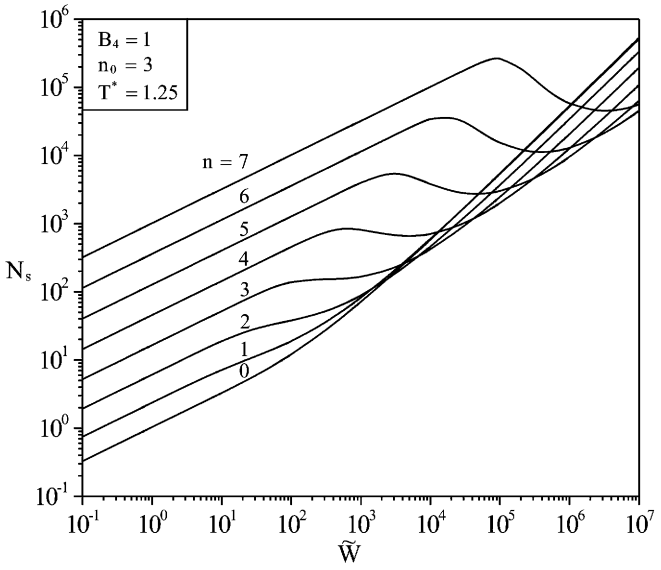

Fig. 10. Effect of the dimensionless pumping power $\widetilde{W}$ and complexity n on the entropy generation ratio N_s for the dendritic structure of Fig. 7.

$B_4 = 1$, $n_0 = 3$ and $T^* = 1.25$. The figure shows again that complexity can be profitable at larger pumping power values and because of that an envelope curve for minimum entropy generation number exists.

5. Conclusions

In this paper, we propose a new method for thermodynamic optimization to several classes of simple flow systems consisting of T- and Y-shaped assemblies of ducts, channels and streams. In each case, the objective was to identify the geometric configuration that maximized performance subject to several global constraints. The thermodynamic performance maximization is achieved by minimization of the entropy generated in the system. The boundary condition is fixed temperature of the channel wall. The flow is laminar and fully developed (Hagen–Poiseuille).

The relatively simple constructs, and the various formulation of the global performance maximization problem were chosen intentionally in order to stress the most important features in the method. The maximization of the thermodynamic performance in pure fluid flow, through the minimization of the global flow resistance, is a particular case of this method. The emergence of geometric structure is a result of the consistent maximization of performance subject to constraints and every detail of the optimal flow geometry was a result of the pursuit of better global performance subject to global constraint.

Another important feature illustrated by these examples is the robustness of the optimized design for $\widetilde{D}$. The optimal ratio of the channel thickness ($\widetilde{D} = D_1/D_0$) is completely independent of the rest of the geometric parameters and global constraints. This simplifies the design of future and more complex systems, and, at the same time, insures a near-optimal performance of existing systems the structures of which may deviate from the originally intended design.

Throughout these series of examples we show that the optimized geometry has the effect of "partitioning" optimally certain features of the system. Optimal partitioning, or optimal allocation of constrained quantities is a by-product of the optimization of flow geometry. It is encountered every time global performance is maximized: optimal allocation is another way of interpreting the special optimization of the flow arrangement, i.e. *the optimal distribution of imperfection* [2].

More fundamentally, the sequence in which the examples were presented in this paper holds an important message for future applications of the method. We started with these examples because they are the simplest, but they can serve as a base of more complicated design configurations. Moreover, the new criterion (pursuing two objectives simultaneously) is an instrument for evaluating and comparing the performance characteristics of different design configurations for the same global constraints [19,22–24].

Acknowledgement

V.D. Zimparov expresses his deep gratitude to the Fulbright Commission for the financial support of his work at Duke University through the Fulbright Grant 04-21-01.

References

[1] A. Bejan, Advanced Engineering Thermodynamics, second ed., Wiley, New York, 1997.
[2] A. Bejan, Shape and Structure, from Engineering to Nature, Cambridge University Press, Cambridge, UK, 2000.
[3] Y. Chen, P. Cheng, Heat transfer and pressure drop in fractal tree-like microchannel nets, Int. J. Heat Mass Transfer 45 (2002) 2643–2648.
[4] D.V. Pence, Reduced pumping power and wall temperature in microchannel heat sinks with fractal-like branching channel networks, Microscale Thermophys. Eng. 6 (2002) 319–330.
[5] A. Bejan, I. Dincer, S. Lorente, A.F. Miguel, A.H. Reis, Porous and Complex Flow Structures in Modern Technologies, Springer, New York, 2004.
[6] Z.Z. Xia, Z.-X. Li, Z.-Y. Guo, Heat conduction optimization: high conductivity constructs based on the principle of biological evolution, in: Twelfth Int. Heat Transfer Conf., Grenoble, France, 18–23 August 2002.
[7] D. Tondeur, L. Luo, U. d'Ortona, Optimisation des transferts et des des materiaux par l'approche constuctale, Entropie 30 (2000) 32–37.
[8] A. Rivera-Alvarez, A. Bejan, Constructal geometry and operation of adsorption processes, Int. J. Therm. Sci. 42 (2003) 983–994.
[9] M.-O. Coppens, Y. Cheng, C.M. van den Bleek, Controlling fluidized bed operation using a novel hierarchical gas injection system, Paper 304d, AIChE Annual Meeting, Dallas, TX, October 31–November 5, 1999.
[10] J.V.C. Vargas, A. Bejan, Thermodynamic optimization of internal structure in a fuel cell, Int. J. Energy Res. 28 (2004) 319–339.
[11] S.M. Senn, D. Poulikakos, Laminar mixing, heat transfer and pressure drop in tree-like microchanel nets and their application for thermal management in polymer electrolyte fuel cells, J. Power Sour. 130 (2004) 178–191.
[12] J.V.C. Vargas, J.C. Ordonez, A. Bejan, Constructal flow structure for a PEM fuel cell, Int. J. Heat Mass Transfer 47 (2004) 4177–4193.
[13] A. Bejan, L.A.O. Rocha, S. Lorente, Thermodynamic optimization of geometry: T- and Y-shaped constructs of fluid streams, Int. J. Therm. Sci. 30 (2000) 949–960.
[14] A. Bejan, M.R. Errera, Convective trees of fluid channels for volumetric cooling, Int. J. Heat Mass Transfer 43 (2000) 3105–3118.
[15] S. Lorente, W. Wechsatol, A. Bejan, Tree-shaped flow structures designed by minimizing path lengths, Int. J. Heat Mass Transfer 45 (2002) 3299–3312.
[16] W. Wechsatol, S. Lorente, A. Bejan, Tree-shaped insulated designs for the uniform distribution of hot water over an area, Int. J. Heat Mass Transfer 44 (2001) 3111–3123.
[17] W. Wechsatol, S. Lorente, A. Bejan, Development of tree-shaped flows by adding new users to existing networks of hot water pipes, Int. J. Heat Mass Transfer 45 (2002) 723–733.
[18] W. Wechsatol, S. Lorente, A. Bejan, Optimal tree-shaped networks for fluid flow in a disc-shaped body, Int. J. Heat Mass Transfer 45 (2002) 4911–4924.
[19] W. Wechsatol, S. Lorente, A. Bejan, Dendritic heat convection on a disc, Int. J. Heat Mass Transfer 46 (2003) 4381–4391.
[20] A. Bejan, Dendritic constructal heat exchanger with small-scale crossflows and larger-scales counterflows, Int. J. Heat Mass Transfer 45 (2002) 4607–4620.
[21] A.K. da Silva, S. Lorente, A. Bejan, Constructal multi-scale tree-shaped heat exchanger, J. Appl. Phys. 96 (2004) 1709–1718.
[22] V. Zimparov, A.K. da Silva, A. Bejan, Thermodynamic optimization of tree-shaped flow geometries, Int. J. Heat Mass Transfer 49 (2006) 1619–1630.
[23] A. Bejan, S. Lorente, La Loi, Constructale, L'Harmattan, Paris, 2005.
[24] A. Bejan, S. Lorente, The constructal law and the thermodynamics of flow systems with configuration, Int. J. Heat Mass Transfer 47 (2004) 3203–3214.